Silicon (2023) 15:4285–4296
https://doi.org/10.1007/s12633-023-02329-2

ORIGINAL PAPER

Simulation-based Study of Super-Nernstian pH Sensor Based on Doping-less Tunnel-field Effect Transistor

Zuber Rasool[1] · S. Intekhab Amin[1] · Lubna Majeed[1] · Ishrat Bashir[1] · Anjar Seraj[1] · Sunny Anand[2]

Received: 17 October 2022 / Accepted: 1 February 2023 / Published online: 23 February 2023

Abstract

In this work, we have simulated doping less tunneling field-effect transistor (DL-TFET) based pH sensor which can detect the pH variation in an aqueous (electrolyte) medium. The source-sided underlapped technique is employed to achieve better sensitivity. The simulated results were extracted with the help of the software package TCAD-Silvaco. In this work, we have compared the pH sensing capabilities of both conventionally doped TFET (C-TFET) and DL-TFET having the same configuration. Result suggests that the sensitivity of DL-TFET is equal to that of C-TFET. Since DL-TFET already exhibits superiority over C-TFET in terms of better immunity against random doping fluctuations (RDF), low fabrication cost and complexity, it can be used as a better alternative to C-TFET based ISFETs. Furthermore, in this work, we have discussed and demonstrated how the performance and sensitivity of the DL-TFET device can be further increased by the use of low energy band materials like germanium in the source region and high K dielectric materials like Al_2O_3 as a sensitive oxide layer underneath the underlapped region. The voltage sensitivity achieved by DL-TFET in this work is 312 mV/pH which surpasses the Nernst limits by more than 5 times.

Keywords Charge plasma · DL-TFET · Electrolyte · ISFET · Nernst limit · pH sensor · TCAD · Tunnel FET

1 Introduction

Ion Sensitive field effect transistor (ISFETs) are widely used in sensing operations of various biological species and chemical compounds. It was first introduced by Bergveld in 1970 [1]. Since then, FET based sensing devices have been drawing huge attraction from researchers. They have various advantages like label-free detection, portability, reusability, low power consumption, low cost, fast detection and compatibility with the current CMOS technology [1–5]. Most of these devices work on the principle that target charged biomolecules or chemical compounds cause a shift in surface potential (field gating effect) which in turn results in the variation of threshold voltage (V_T), due to which drain current (I_d) also varies and these variations in either of the parameters can be used a criterion for sensing of various biological species and chemical compounds [6–11]. Conventional FET devices like MOSFETs suffer from the issue of minimum sub-threshold slope limitation and an increase in short channel effects due to continuous downscaling. Theoretically the subthreshold swing of MOSFETs is limited to 60 mV/dec [12]. The sensitivity of conventional MOSFET based ISFET devices revolves around the Nernst limit [7, 8, 13]. The Nernst limit states that the maximum sensitivity that can be achieved by ISFETs is nearly 59 mV/pH at room temperature. However, many researchers employed various structural modifications and improvements to overcome the sensitivity of their devices beyond the Nernstian limit [6, 7, 10, 14–16]. Higher sensitivity signifies better detection capability of the device even with lower concentration of analyte samples.

Tunnel field effect transistor (TFET) is one of the emerging nano-electronic devices. Tunnel field effect transistors (TFET) are gaining popularity due to superiority over MOSFET as they can have a low subthreshold swing of less

✉ S. Intekhab Amin
samin@jmi.ac.in

Zuber Rasool
rasoolzuber3@gmail.com

Lubna Majeed
lubmaj234@gmail.com

Ishrat Bashir
Ishratbashir00@gmail.com

Anjar Seraj
anjarseraj98@gmail.com

Sunny Anand
sunnyanand.42@gmail.com

[1] Jamia Millia Islamia University, New Delhi, India

[2] Amity University Uttar Pradesh, Noida, India

than 60 mV/dec and it also possesses low off-state leakage current [17–19]. TFET is also immune to short channel effects due to the tunneling barrier [20]. Sarkar et al. [19]. in their work showed that Tunnel field effect transistor-based bio-sensor shows higher sensitivity than the Conventional-FET counterparts as well as they have comparatively lesser response time due to band to band tunneling phenomenon. The bio-molecules or chemical compound reacts with the sensitive oxide layer and result in variation of capacitance as well as charge densities at oxide surfaces, resulting in the change of tunneling width of the TFET device, which in turn changes the tunneling rate of electrons, hence variations in tunneling current and shift in threshold voltages can be observed. So, these parameters can be used for recognizing the specific bio-species or chemical compound. Conventional TFET (C-TFET) consist of a P-I-N structure having heavily doped P and N regions with intrinsic semiconductor-based channel. Although the issue of minimum achievable sub-threshold slope can be resolved by using a conventional TFET device, it still suffers from issues like Random doping fluctuations (RDF) [21] and high fabrication cost and complexity [22, 23]. Random doping fluctuations are caused majorly due to the trapping and de-trapping of charge carriers at the interface of tunneling junction resulting in higher OFF state current, it is dominant in highly scaled TFET devices [21]. These problems can be solved by Doping-less Tunnel field effect transistors (DL-TFET), it was first introduced by Jagadesh et al. [22]. In Doping-less TFET work function of source and drain electrodes are used for the formation of heavily doped P and N regions on intrinsic silicon body [22, 23]. The functionality of DL-TFET is similar to that of conventional-TFET but with the benefits of reduced fabrication cost and immunity against RDF. A better performing derivative of DL-TFET having high on-state current was introduced by Anand et al. [23] in which they used a dual electrode-based doping less TFET device. As DL-TFET definitely has superiority over Conventional doped TFET, it can be used as an alternative for C-TFET based bio-sensors. Although analysis of Dielectrically Modulated Doping Less Tunnel-FET based biosensor is already done in previous works [24, 25]. But still, there is a requirement for the detailed study of DL-TFET pH sensing device which is sensitive to aqueous environment (electrolyte). As C-TFET device which is sensitive to pH variations is already analyzed by Dwivedi et al. [26] their work showed that TFET based pH sensors can achieve sensitivity beyond the Nernst limit. Therefore, in this work, we have investigated a DL-TFET based pH sensing device and compared it with C-TFET counter-parts on various parameters like voltage sensitivity, current sensitivity, etc. With the help of computer-based simulation software called TCAD-Silvaco [27], we have demonstrated how the pH of an electrolyte in an aqueous medium can be detected by using source-sided underlapped DL-TFET. The electrolyte is placed in the source sided underlap region of both conventional and doping less TFET and a detailed comparison of both devices were done. We found that doping less TFET based pH sensor shows the same sensitivity (slightly higher) than that of conventional TFET based pH sensing devices with obvious benefits of reduced fabrication cost and immunity against RDF. It is evident from the work [28] that the use of low energy bandgap materials like germanium as a source substrate increases the device performance by increasing the On-state current. Some previous works also suggest that the use of high-K dielectric material when used as the oxide layer, improves the sensitivity of the device [6, 8]. So, we have investigated the effects of replacing source material with low energy-band (germanium) materials and sensing oxide layer to high-K dielectric materials (Al_2O_3) in our DL-TFET based sensor. The sensitivity obtained by our device surpasses the Nernst limit by more than 5 times.

2 Simulation and Setup

For simulation, we have used ATLAS (Silvaco) TCAD tool [27]. The gate length (L_g) is taken to be 50 nm. The electrolyte has been taken under both top and bottom source sided underlapped region to get attain more sensitivity. The length of under-lap region (L_{un}) is taken to be 30 nm which covers the tunneling region. As the tunneling rate of DL-TFET depends on the spacing between source and the gate electrode, it is kept 30 nm by taking into consideration that we have to increase the device sensitivity without causing much damage to the drain current. The thickness ($T_{sen\text{-}ox}$) of insulator oxide (SiO_2) is kept to be 3 nm which is sufficient enough to restrict mobilization of bio-molecules or chemical ions. For doping less TFET work function of source and drain electrode work function are taken to be 5.93 eV and 3.9 eV as same as work function of platinum and hafnium metal [22, 23]. The thickness of the silicon (T_{si}) body is kept to be 10 nm. The Doping less TFET design used in this work consist of dual electrode as it shows more on state current than single electrode-based DL-TFET [23]. The calibration is also done according to the work [23]. The doping concentration of the source and drain region are considered to be 10^{20} cm^{-3} and 5×10^{18} cm^{-3} respectively for Conventional doped TFET, otherwise all the configurations of DL-TFET and C-TFET are kept to be similar. The monovalent electrolyte with an equal amount of positive (cation) and negative ion (anion) in an aqueous environment can be modeled as an intrinsic semiconductor having zero energy band gap and permittivity of water (80) [26, 29–32]. The similarity between the Poisson-Boltzmann equation for ions of electrolyte and electrons-holes pairs in an intrinsic semiconductor is used for the modeling of electrolyte

as a semiconductor in the simulation [26, 29–32]. As per S. Koneshan et al. [33], the mobility of Na^+ and Cl^- for 1 mmol/L concentration of NaCl solution will be 4.98×10^{-4} cm^2 /V s and 6.88×10^{-4} cm^2 /V s. So, we used these values as the maximum velocity of holes and electrons respectively in semiconductor (electrolyte). We have also used the electric double layer model as reported in works [31, 32]. Electric double is an electrically passive layer formed by immobile ions near the oxide-electrolyte interface. The thickness (T_{stern}) of this layer is considered to be 4 nm and has a constant permittivity of 2. The thickness of the cavity region for filling electrolyte (T_{el}) is taken to be 20 nm as shown in Fig. 1 (a) and (b). Models used for simulation are non-local band to band tunneling to capture band to band tunneling, Fermi Dirac statistics model, Shockley–Read–Hall recombination model, Band gap narrowing (BGN) and concentration and field dependent mobility model are used. The relationship between pH of electrolyte and surface potential (ψ_0) is given by combination of Gouy-Chapman-stern model and Site Binding theory [34] (Eq. 1).

$$\frac{d\psi_0}{dpH} = 2.303\alpha kt/q \tag{1}$$

where ψ_0 being the surface potential at oxide/electrolyte interface, α is sensitivity parameter having value between 0 and 1 depending on value of buffer capacitance of gate dielectric and the concentration of electrolyte solution, k is Boltzmann's constant and t is temperature.

Bousse et al. [35] used site binding theory and electric double layer to develop relationship between surface potential and pH for oxide surface as given by Eq. (2).

$$\psi_0 = -2.303\frac{kt}{q}\frac{\beta}{1+\beta}(pH - pH_{pzc}) \tag{2}$$

$$pHpzc = -log_{10}\sqrt{\frac{K_a}{K_b}} \tag{3}$$

$$\beta = q\,N_s\frac{\eta}{C_{eq}V_{th}} \tag{4}$$

$$C_{eq} = \frac{C_{st}\times C_{dl}}{C_{st}+C_{dl}},\ \eta = 2\sqrt{\frac{K_b}{K_a}} \tag{5}$$

$$C_{dl} = \sqrt{\frac{2Z_K^2\varepsilon_w q n_0}{V_{th}}} \tag{6}$$

$$n_0 = n_i = q_{eff}\times N_{avo} \tag{7}$$

β is a constant can be calculated by Gouy-Chapman stern model as mentioned in Eq. (4), $\frac{kt}{q} = V_{th}$ is thermal voltage (26 mV at room temperature) and pH_{pzc} is the pH value at which the oxide surface acts neutral or surface charge density is zero given by Eq. (3). K_a and K_b represents acid and base disassociation constants of the oxide surface whose values are given in Table 1. N_s is amount of site binding charge per unit area (values shown in Table 1). C_{dl} represents double layer capacitance and is given by Eq. (6) and C_{st} is known as stern capacitance and it have a constant value of 0.2 F/m^2.ε_w represents the dielectric constant of water (80), Z_k is the valency of K^{th} ion, here it is taken to be one due to consideration that solution contain only NaCl and both ions Na^+ and Cl^- have valency of 1 and n_0 is ion concentration of electrolyte which is same as intrinsic carrier density, so it can be written as Eq. (7). q_{eff} and N_{avo} mentioned in Eq. (7) represents effective ionic charge and Avogadro's number (6.023×10^{23}/mol) respectively. The variation of interface

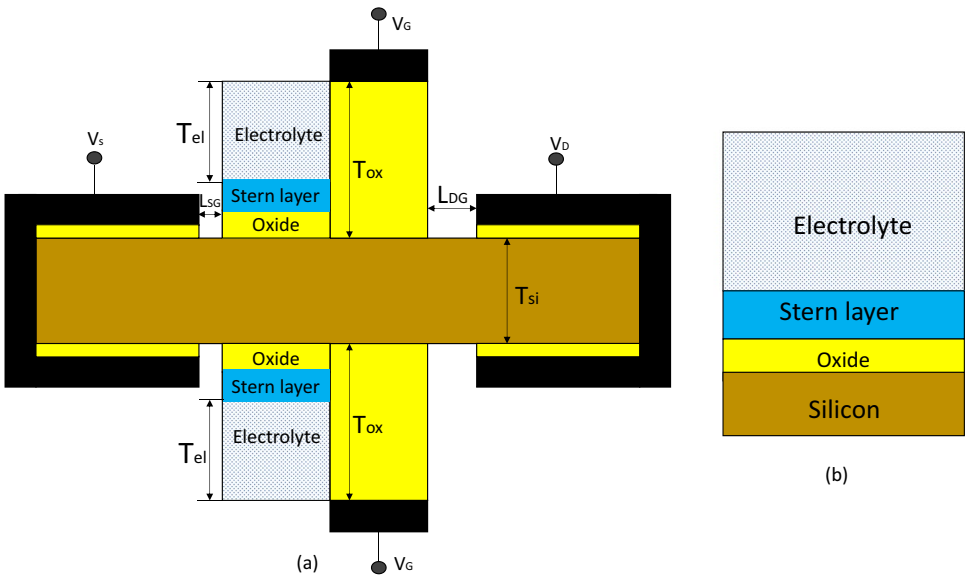

Fig. 1 (**a**) Top view of our proposed dual electrode base DL-TFET ba sed pH sensor with dual underlap lap region. (**b**) Enlarged view of sensitive area over the channel

Table 1 Values of parameters for SiO_2 and Al_2O_3

Symbol	SiO_2	Al_2O_3	References
ε_r	3.9	14	[36]
N_S (cm^{-2})	5.10^{14}	8×10^{14}	[36]
K_a	10^{-6}	10^{-10}	[36]
K_b	10^{2}	10^{-6}	[36]
Band gap (eV)	9	8.8	[6]

charge density at the semiconductor channel and oxide interface for the ISFETs depends on the change in surface potential of the oxide/fluid interface and is shown by Eq. (8).

$$\Delta\sigma_{sc} = -C_{ox}\Delta\psi_0 = -\frac{\varepsilon_0\varepsilon_{ox}}{t}\Delta\psi_0 \tag{8}$$

$\Delta\sigma_{sc}$ being the interface charge density, C_{ox} is oxide capacitance, $\Delta\psi_0$ is change in surface potential at the oxide/electrolyte interface, t is thickness of oxide layer, and ε_{ox} is relative permittivity of oxide layer.

As from Eq. (2) change in surface potential ($\Delta\psi_0$) can be calculated and with the help of Eq. (8) we can obtain the values of interface charge density for the corresponding pH value and these values of interface charge density at the channel/oxide interface can be used as a parameter for modeling pH values in the simulation, and we have employed the same. The surface charge density in the work is calculated by assuming solution to be 0.001 × PBS.

3 Results and Discussions

Figure 2(a) and (b) shows variation of drain current (I_{ds}) vs gate voltage (V_g) (transfer characteristics) curve for pH varying from 1 to 10 for C-TFET and DL-TFET respectively. In TFET devices the drain current is proportional to tunneling probability and that depends on the exponential variation of the gate voltage (V_g) [18]. It is observed that current in both conventional TFET and DL-TFET is nearly same as shown in Fig. 2(c). DL-TFET shows slightly less current than the C-TFET for equivalent pH values because the current in DL-TFET depends on the spacing between source and gate region, generally it is kept in the order of 3–5 nm [22, 23] but to gain more sensitive area (underlap region) we have increased it to 30 nm (total tunneling region), hence the maximum current obtained by DL-TFET is slightly less than that of C-TFET (Fig. 2(c)). As the pH increases the interface charge density becomes more negative.

resulting in the widening of the tunneling width which in turn decreases the band-to-band electron tunneling rate (BTBT) of the device. Therefore, the decrement of drain current is observed with increase in the pH value for both TFET devices. The transfer characteristics with increase in pH for both devices at $V_{ds} = 1$ V can be observed by the Fig. 2(a) and (b). Figure 2(c) shows the comparison of transfer characteristics (I_d vs V_g) curve between C-TFET and DL-TFET based device for a pH value of 1 and 10. The variation of energy band gap for both C-TFET and DL-TFET is shown in the Fig. 2(d) and (e). A cutline is made at 1 nm below the oxide-channel interface at $V_g = 3$ V and $V_{ds} = 1$ V and energy levels of conduction band and valence is extracted. Figure 2(d) and (e) shows the variation of conduction band (CB) and valence band (VB) for pH values of 1, 5 and 10 for C-TFET and DL-TFET respectively. As the pH value increases from 1 to 5 and then to 10, increase in the bending of energy band is observed which causes widening of tunneling width which in turn decreases the BTBT rate and hence lower value of drain current (I_{ds}) is observed.

The most important parameters to evaluate the sensing capacity of a biosensor or ISFET is voltage sensitivity (S_V) and current sensitivity (S_I). Conventionally in FET based biosensors the sensitivity of the device is calculated as a shift in threshold voltage or ratio of change of drain current at a specific gate voltage. We have calculated current and voltage sensitivities as per work done by Liu et al. [7]. Voltage sensitivity (S_V) is calculated for a constant value of drain current (I_{ref}). For a specific value of drain current (I_{ref}) the corresponding responsive gate voltage (V_R) is obtained and the shift in that gate voltage (ΔV_R) with respect to a pH value can be used to find voltage sensitivity (S_V). In our work we have calculated ΔV_R for a specific value of I_{ref} as ΔV_R (at any pH) = V_R (at any pH)—V_R (at pH = 1). In Fig. 3(a) and (b) the curve of ΔV_R vs pH for reference values of drain current (I_{ref}) _ 10^{-9} A, 10^{-10} A, 10^{-11}A, 10^{-12} A and 10^{-13}A is shown. The voltage sensitivity (S_V) attained by C-TFET device for I_{ref} values of 10^{-9} A, 10^{-10} A, 10^{-11}A, 10^{-12} A and 10^{-13}A are 224.85 mV/pH, 226.4 mV/pH, 226 mV/pH, 224.24 mV/pH and 218.75 mV/pH respectively whereas the voltage sensitivity (S_V) achieved by DL-TFET device for I_{ref} values of 10^{-9} A, 10^{-10} A, 10^{-11}A, 10^{-12}, 10^{-13}A are 240 mV/pH, 238 mV/pH, 236.61 mV/pH, 234.97 mV/pH and 223.68 mV/pH respectively. The current sensitivity (S_I) represents ratio of change of drain current with respect to a pH value for a specific gate voltage (V_{ref}). Therefore, the sensitivity (S_I) at specific gate voltage (V_{ref}) is calculated as $S_I = (I_{ds}$ (at any pH) $-I_0)/ I_0$ where I_0 is the drain current obtained at pH = 10. Figure 3(c) and (d) shows the current sensitivity of C-TFET and DL-TFET devices respectively. From Fig. 3(c) and (d) it can be seen that the maximum current sensitivity achieved by both devices is around 10^8 for pH = 1 and the minimum current sensitivity is nearly greater than 10 for DL-TFET at pH = 9 while taking current at pH = 10 as reference (I_0). The current sensitivity depends on the range of pH, it is low for consecutive pH values and increases as we increase the pH difference. The maximum current sensitivity for C-TFET is achieved for gate voltage (V_{ref}) of 2 V and for DL-TFET same is achieved for gate

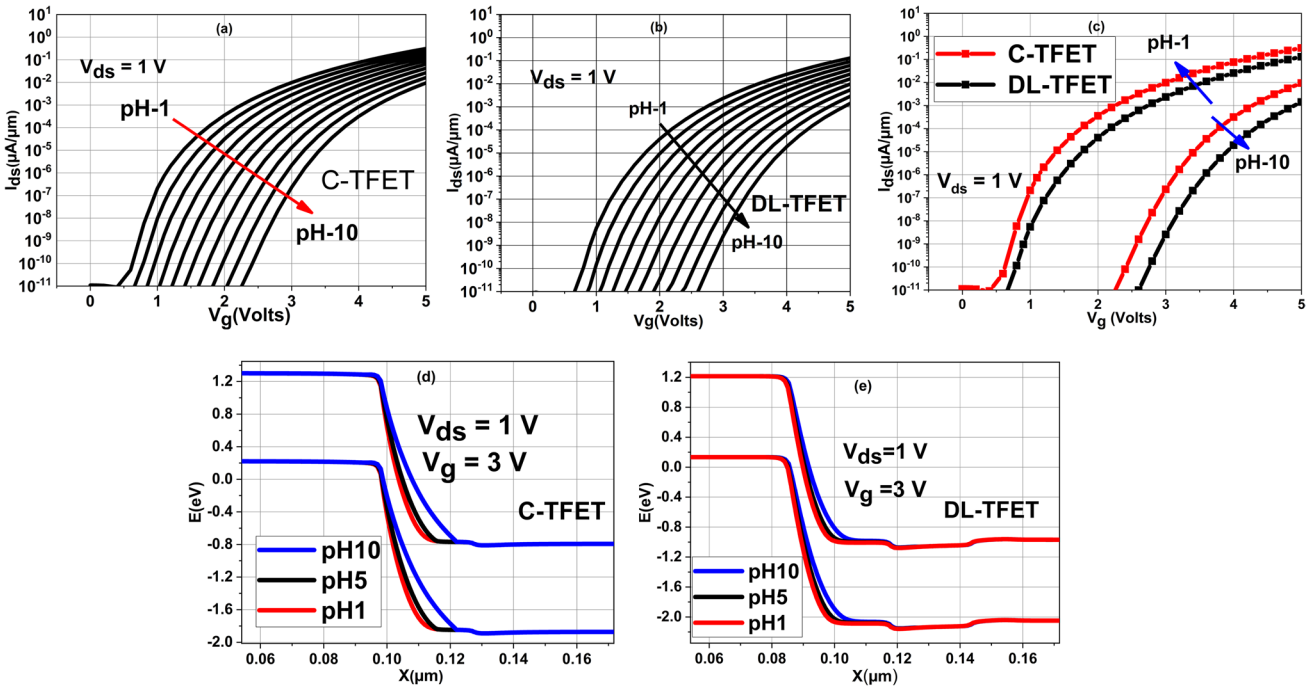

Fig. 2 Drain current (I_{ds}) vs. gate voltage (V_g) as a function of pH varying from 1 to 10 (**a**) Conventional doped tunnel field effect transistor (TFET) (**b**) Doping less tunnel field effect transistor (DL-TFET) (**c**) Comparison of drain current vs. gate voltage for C-TFET and DL-TFET device for pH values of 1 and 10. Variation of conduction band and valence band energy levels for pH = 1,5 and 10 for (**d**) C-TFET and (**e**) DL-TFET

voltage (V_{ref}) of 2.5 V. This can be also viewed as that the DL-TFET operates at slightly higher gate voltage than the C-TFET to achieve equivalent drain current. The current sensitivity decreases if gate voltage increases beyond 2 V for C-TFET and 2.5 V for DL-TFET (Fig. 3(c) and (d)) due to saturation in BTBT rate. The sensitivity of DL-TFET surpasses the Nernst limit (59.2 mV/pH) up to 4 times owing to the band to band tunneling phenomenon. The surface charge variations (pH variations) results in higher threshold voltage variations than the inversion mode devices due to BTBT mechanism (Fig. 3(e)), hence the sensitivity greater than Nernst limit is achieved. The voltage sensitivity also holds good linearity for both C-TFET and DL-TFET, so it is better parameter than change in drain current (S_I) to determine change in pH values. The maximum electron tunneling rate for both devices at $V_g = 2.5$ V and $V_{ds} = 1$ V for every pH value ranging from 1 to 10 is extracted 1 nm below the oxide channel interface and results are shown in Fig. 3(e). The tunneling rate achieved by DL-TFET device is lesser than that of the C-TFET device which can also be validated by the lower drain current comparison of both devices as depicted in the Fig. 2(c). From all these results we can conclude that DL-TFET can be used as a better alternative for C-TFET in sensing applications. The variation in the current with pH can also be visualized by the change in electron concentration and potential contour of the sensitive area (channel region below the underlapped region). The Fig. 4(a) and (b) shows the electron concentration of DL-TFET for pH = 1 and 10 for $V_{ds} = 1$ V and $V_g = 2.5$ V (as maximum variation is observed at 2.5 V). The electron concentration for pH = 1 varies from 10^4 cm^{-3} to 10^{18} cm^{-3} in the sensitive region whereas for pH = 10 electron concentration varies from 10^4 cm^{-3} to 10^{16} cm^{-3} and the area having low concentration of electrons (10^4 cm^{-3} to 10^{10} cm^{-3}) is more for pH = 10 than pH = 1. Figure 4(c) and (d) shows the potential variation in DL-TFET device for pH = 1 and pH = 10 for $V_g = 2.5$ V. It can be clearly seen by Fig. 4(c) and (d) that for pH = 1 surface potential (ψ) is greater than 1 V for the wide area in the sensitive channel region whereas it is below 1 V all over the sensitive channel area for pH = 10. The distribution of

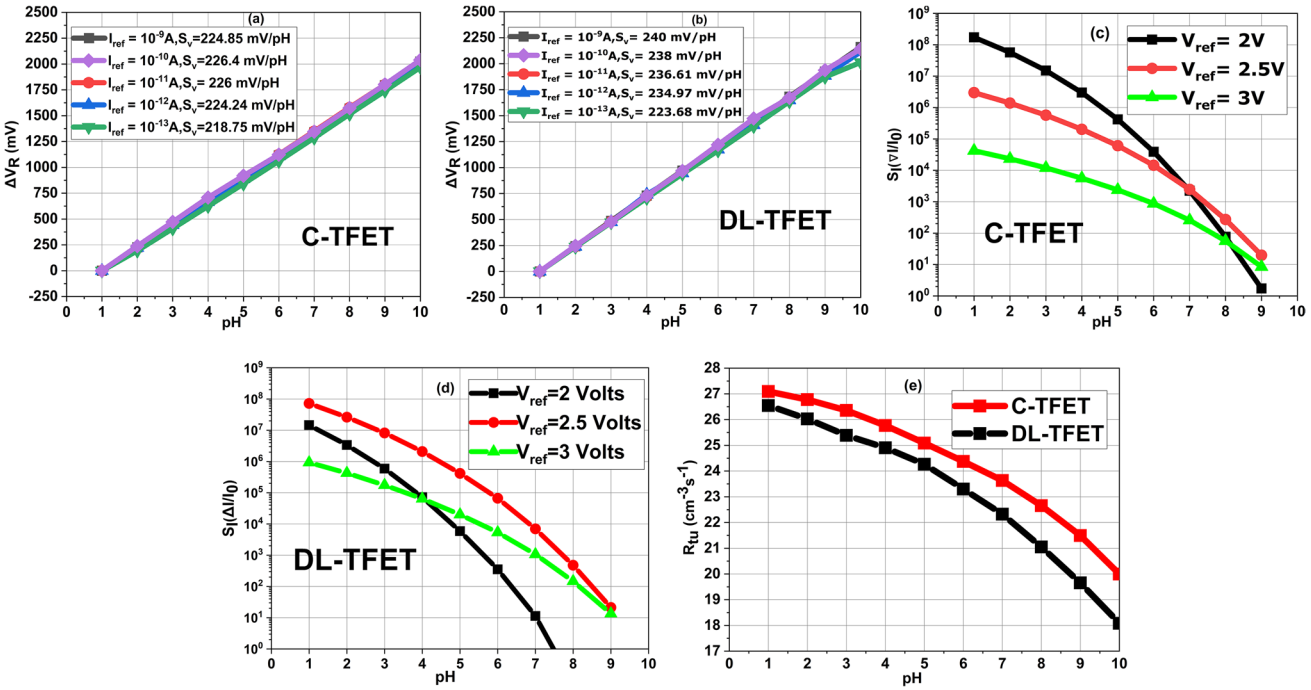

Fig. 3 Variation of responsive gate voltage (ΔV_R) with pH for drain current (I_{ref}) of 10^{-9} A, 10^{-10} A, 10^{-11} A, 10^{-12} A and 10^{-13} A and variation of S_I with pH for gate voltage (V_{ref}) of 2 V, 2.5 V and 3 V (**a**) ΔV_R in C-TFET (**b**) ΔV_R in DL-TFET (**c**) S_I in C-TFET (**d**) S_I in DL-TFET (**e**) Maximum band to band electron tunneling rate (R_{tu}) rate with change in pH values for C-TFET and DL-TFET

potential across the channel other than the region underneath the underlap region is similar for both pH values of 1 and 10.

As we have already achieved sensitivity way beyond Nernst limit, we are further going to discuss how the sensitivity, device performance and stability can further be increased in the DL-TFET device. It is evident from the work [28] that use of low energy band gap materials like germanium instead of silicon in the source region of DL-TFET can improve the drain current (I_{ds}). The lower energy band of the material facilitates better tunneling of electron, which in turn gives higher BTBT rate provides enhanced value of on state drain current. So, we investigated the same and also studied impact of using low energy band material on the sensitivity of our DL-TFET based device. We replaced the source region with germanium keeping electron concentration same as 1.5×10^{15} cm^{-3} and then calculated various parameters and compared it with silicon source-based DL-TFET.

Figure 5(a) shows the variation of transfer characteristic (I_{ds} vs V_g) with pH (pH = 1 to 10) for germanium source-based DL-TFET. Figure 5(b) shows the comparison of the drain current vs gate voltage for the silicon and germanium-based source variants of DL-TFET device at pH = 1 and pH = 10. Overall increment in drain current is observed with the use of germanium material instead of Silicon in the source region. This obviously improves the device characteristics, but our main concern lies in the sensitivity whether it is improved or not. So, we calculated both current sensitivity (S_I) and voltage sensitivity (S_V) of the device. Figure 5(c) shows the variation of responsive gate voltage (ΔV_R) vs pH of DL-TFET device with germanium as source material. The voltage sensitivities obtained at drain current (I_{ref}) = 10^{-9} A, 10^{-10} A, 10^{-11}A, 10^{-12}A and 10^{-13}A are 278 mV/pH, 270 mV/pH, 265.19 mV/pH and 256 mV/pH. Overall increment in voltage sensitivity of more than 30 mV/pH is observed by replacing the source material with germanium. Figure 5(d) shows the ratio of change in drain current (S_I) with respect to pH changing from 1 to 10, the S_I is more than 10 for consecutive pH change at 2.5 V and its maximum value is 1.29×10^8 calculated for pH = 1 by taking current at pH = 10 as reference current (I_0). Figure 5(e) shows comparison of the ratio of change in drain current (S_I) for DL-TFET device with silicon and germanium-based

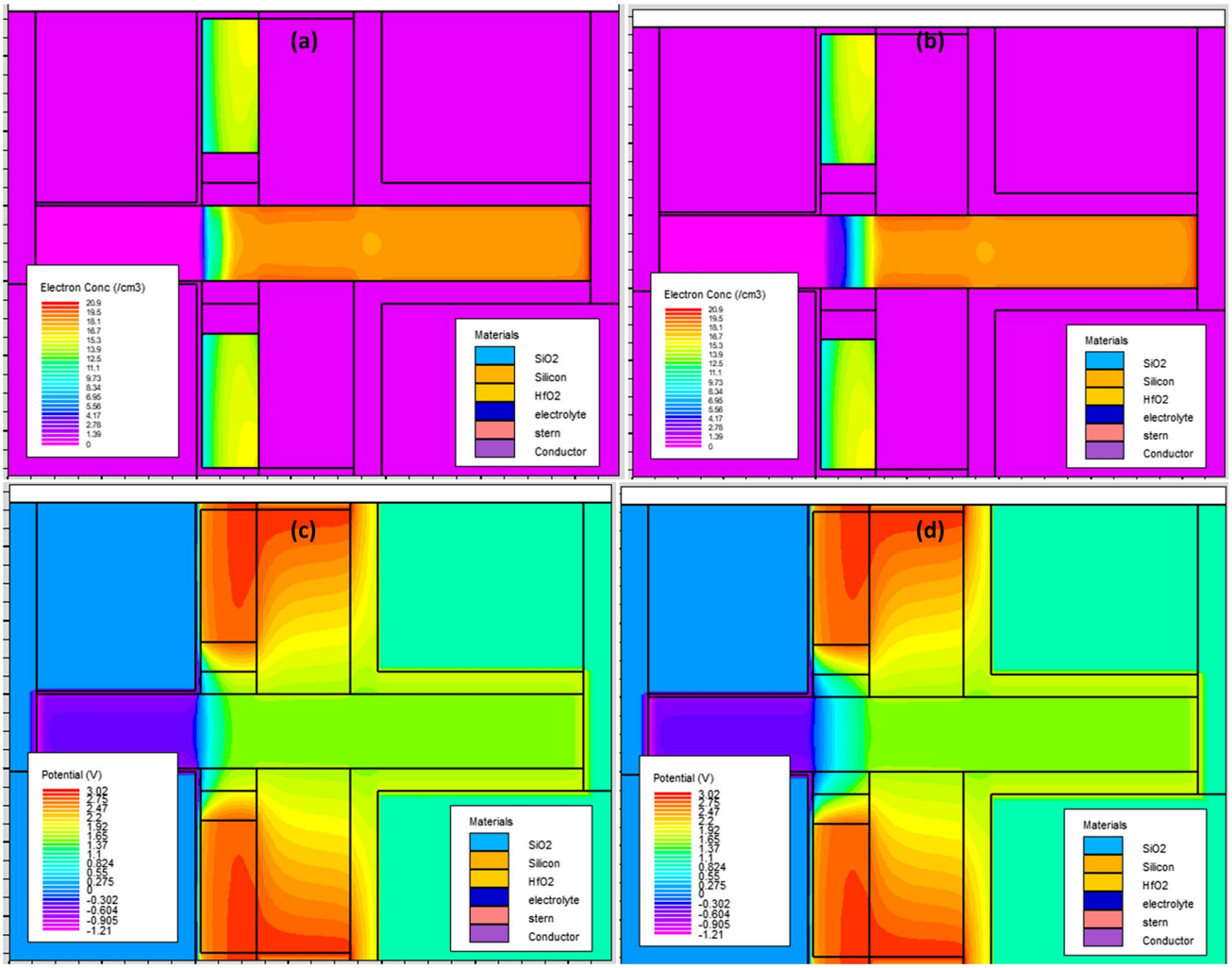

Fig. 4. 2D contours showing electron concentration of DL-TFET device for (**a**) pH = 1, (**b**) pH = 10. 2D contours showing surface potential for DL-TFET device for (**a**) pH = 1, (**b**) pH = 10. Both results are extracted for a gate voltage $V_{gs} = 2.5$ V where greater variations of drain current are observed

source region at gate voltage (V_{ref}) = 2.5 V and $V_{ds} = 1$ V. S_I obtained by germanium source-based DL-TFET is higher for every pH when compared to silicon source-based DL-TFET (Fig. 5(e)). A Further validation of the improvements in DL-TFET with the use of germanium material is provided by Fig. 5(f), showing comparison of the maximum band to band electron tunneling rate achieved by both germanium and silicon- based DL-TFET device for pH values from 1 to 10 at $V_g = 2.5$ V and $V_{ds} = 1$ V extracted 1 nm below the oxide/channel interface. It can be observed that band to band electron tunneling rate is higher in the germanium source variant of DL-TFET than silicon counter-part. From all these results we can finally interpret that replacing silicon material with germanium in source region not only improves the on-state current but can also increment the device sensitivity with more than 30 mV/pH. From Eq. (8) we conclude that change in interface charge density can be increased by reducing the oxide thickness but reducing the thickness of conventionally used SiO_2 can cripple the device characteristics by increasing leakage current. This leakage increases more when device is operated in ionic fluids. Another approach to increase sensitivity is to use high-K dielectric material as oxide. With the use of high-K dielectric material the oxide thickness can be increased, which could reduce the leakage current and improve the device stability and robustness when used in the ionic fluids [6]. The reactions occurring at the oxide/electrolyte interface for oxides like Al_2O_3, HfO_2 and TaO_2 is similar to that of SiO_2 [29]. Al_2O_3 is generally preferred over other SiO_2 and Si_3N_4 oxides as it can provide more sensitivity and stable characteristics [8, 29]. It allows lower ion diffusion as well [6, 29, 36, 37]. Al_2O_3 also has larger band gap (8.8 eV) which also ensures less leakage current hence results in more stable characteristics [6]. Moreover, Al_2O_3 has larger buffer capacity than SiO_2, hence can result in better sensitivity than

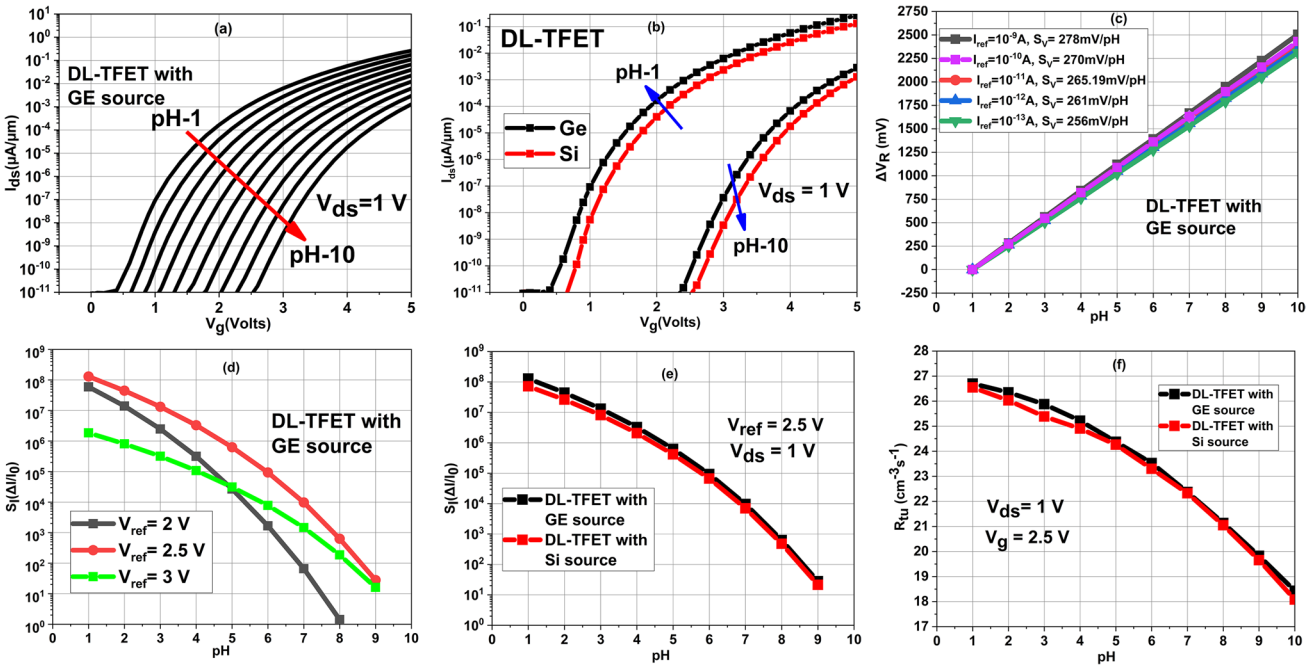

Fig. 5 (**a**) Drain current (I_{ds}) vs. gate voltage (V_g) as a function of pH varying from 1 to 10 for DL-TFET with germanium source. (**b**) Comparison of drain current vs. gate voltage for DL-TFET with germanium and silicon as source material for pH values of 1 and 10 (**c**) Variation of responsive gate voltage (ΔV_R) with pH for drain current (I_{ref}) of 10^{-9} A, 10^{-10} A, 10^{-11}A, 10^{-12} A and 10^{-13}A (**d**) Variation of S_I for DL-TFET with germanium as source material for gate voltage (V_{ref}) of 2 V, 2.5 V and 3 V. (**e**) Comparison of S_I between germanium and silicon material-based DL-TFET device. (**f**) Comparison of maximum band to band tunneling rate for germanium and silicon material based source substrate for DL-TFET device

SiO_2 counter parts. So, we replaced the oxide layer underneath the underlapped region from SiO_2 to Al_2O_3 without changing the capacitance (C_{ox}) of the oxide layer. As oxide capacitance is given as in Eq. 9.

$$C_{ox} = \frac{\varepsilon_0 \varepsilon_{ox}}{t} \tag{9}$$

Originally thickness for SiO_2 was 3 nm, which is now increased to nearly 10.7 nm to yield same oxide capacitance. Fig. 6(a) shows the variation of transfer characteristics with pH of Al_2O_3 based DL-TFET device. Figure 6(b) shows comparison of transfer characteristics of DL-TFET variants having SiO_2 and Al_2O_3 as sensitive oxide layer for pH values of 1 and 10. The Al_2O_3 based device shows lower saturation current for same pH values when compared with SiO_2 counterparts due to the increase overall gap between the channel and gate electrode as we have kept cavity thickness same for both Al_2O_3 and SiO_2 variants. Lowering of threshold voltage is also observed in Al_2O_3 based DL-TFET. The subthreshold slope is higher in Al_2O_3 based DL-TFET. Note that the current can further be increased in Al_2O_3 based DL-TFET by decreasing the oxide thickness. Now coming towards the sensitivities of device, Fig. 6(c) shows the variation of responsive gate voltage ΔV_R with pH for the drain current (I_{ref}) values of 10^{-10} A, 10^{-11} A, 10^{-12} A and 10^{-13} A. The voltage sensitivities obtained for Al_2O_3 based DL-TFET device is 266 mV/pH, 258 mV/pH, 251 mV/pH and 243 mV/pH for I_{ref} of 10^{-10} A, 10^{-11} A, 10^{-12} A and 10^{-13}A respectively. The voltage sensitivity is higher for DL-TFET when Al_2O_3 is replaced by SiO_2 as sensitive oxide layer underneath the electrolyte for same oxide capacitance as that SiO_2. However, the voltage sensitivity and drain current both can be further improved by reducing the thickness of Al_2O_3. Figure 6(d) shows the current sensitivity of Al_2O_3 based DL-TFET device for gate voltage (V_{ref}) of 2 V, 2.5 V and 3 V. The maximum current sensitivity is obtained at 2 V and is less than 10 for consecutive pH variations. From all these results we can conclude that for same oxide capacitance when Al_2O_3 is used instead of SiO_2 lower threshold voltage (V_T) is achieved, significant increase in the maximum voltage sensitivity is also observed (~+25 mV/pH), however decrease in

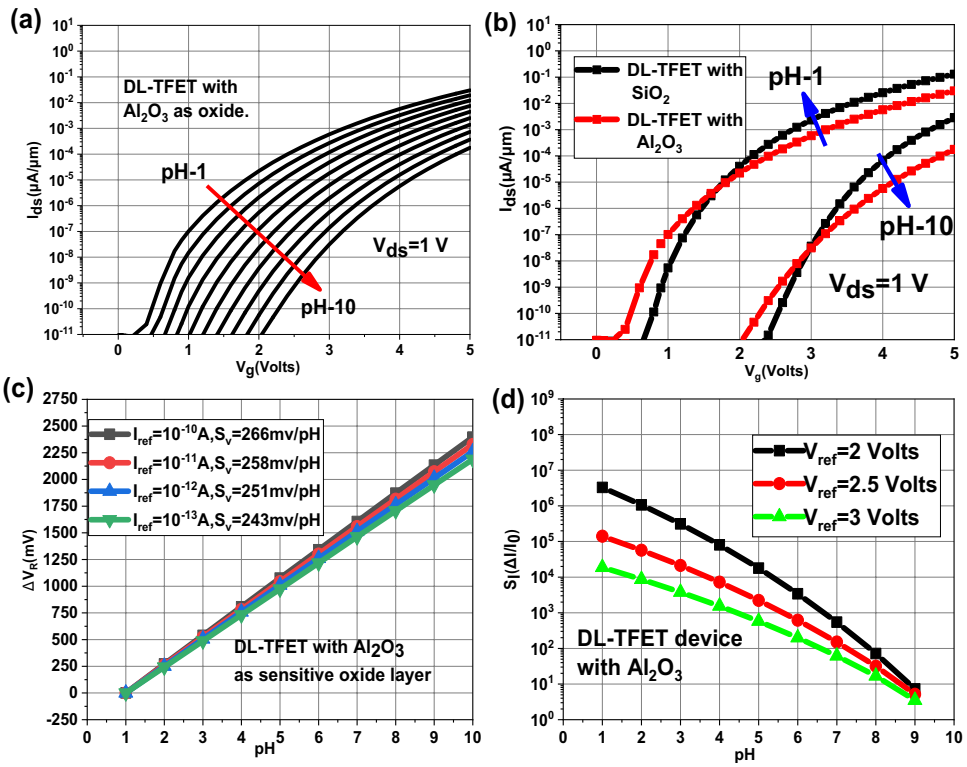

Fig. 6 (**a**) Drain current (I_{ds}) vs. gate voltage (V_g) as a function of pH varying from 1 to 10 for DL-TFET with Al_2O_3 as sensitive oxide layer (**b**) Comparison of drain current vs. gate voltage for DL-TFET with Al_2O_3 and SiO_2 for pH values of 1 and 10 (**c**) Variation of responsive gate voltage (ΔV_R) with pH for drain current (I_{ref}) of 10^{-9} A, 10^{-10} A, 10^{-11}A, 10^{-12} A and 10^{-13} A and (**d**) Variation of S_I with pH for gate voltage (V_{ref}) of 2 V, 2.5 V and 3 V for DL-TFET with Al_2O_3 as underlapped oxide layer

the drain current and decrease in the current sensitivity is also observed. Although the sensitivity achieved by using Al_2O_3 instead of SiO_2 as the sensitive oxide layer underneath the underlapped region is more (266 mV/pH > 238 mV/pH), but the drain current is low. The use of germanium material in the source region not only increases the sensitivity of the device but also increases drain current as well, moreover it can also lower the threshold voltage. So, we finally propose the DL-TFET variant with germanium source and Al_2O_3. This variant will have benefits of lower threshold voltage due of low energy band material, high sensitivity due to both germanium and Al_2O_3 and the low amount of drain current by the use of Al_2O_3 can be compensated by using germanium as a source material. Furthermore, this device also possesses the benefits of low leakage current owing to reduced ion diffusion compared to silicon source-based DL-TFET with SiO_2 as oxide underneath the underlapped region. Figure 7(a) shows the variations of the transfer characteristics with change in pH (1 to 10) of germanium doped source region with Al_2O_3 (10.7 nm) as sensitive oxide layer underneath the underlapped region of the DL-TFET. Figure 7(b) shows comparison between DL- TFET having germanium and silicon as source material with both having Al_2O_3 as sensitive oxide for pH = 1 and 10. With the introduction of low energy level material (germanium) increase in the device drain current can be observed (Fig. 7(b)). Figure 7(c) shows comparison of transfer characteristics at pH = 1 and pH = 10 of DL-TFET device having germanium source and Al_2O_3 oxide with silicon source and SiO_2 based counter parts. Now coming towards the sensitivity of this variant. Figure 7(d) shows the variation of the responsive gate voltage ΔV_R pH for the drain current (I_{ref}) of 10^{-9} A, 10^{-10} A, 10^{-11} A, 10^{-12} A and 10^{-13} A. The voltage sensitivities obtained for this variant of DL-TFET device is found to be 312.2 mV/pH, 298.22 mV/pH, 286 mV/pH, 270 mV/pH and 251.83 mV/pH for I_{ref} of 10^{-9} A, 10^{-10} A, 10^{-11} A, 10^{-12} A and 10^{-13}A respectively. The voltage sensitivity obtained is higher than all other variants mentioned previously in this work. The maximum sensitivity achieved here surpasses the Nernst limit by more than 5 times. Further moving towards the current the sensitivity device (S_I), the ratio of change in drain current with reference current (I_0) assumed to be current at pH = 10 is maximum at gate voltage (V_{ref}) of 2 V and ranges from 10 to 5×10^6 for pH = 9 to pH = 1 respectively as depicted by Fig. 7(e). Finally, the maximum voltage sensitivity achieved by the DL-TFET pH sensor having different configurations is compared and shown by Fig. 8(a). The use of germanium in source side increases the voltage sensitivity of device. The sensitivity is also increased with the use of Al_2O_3 as a sensitive oxide layer below the underlapped region. The highest voltage sensitivity is achieved by the combination of both (use of germanium and Al_2O_3). Figure 8(b) shows the comparison of voltage sensitivity achieved in our work to that of previous work done in the same field.

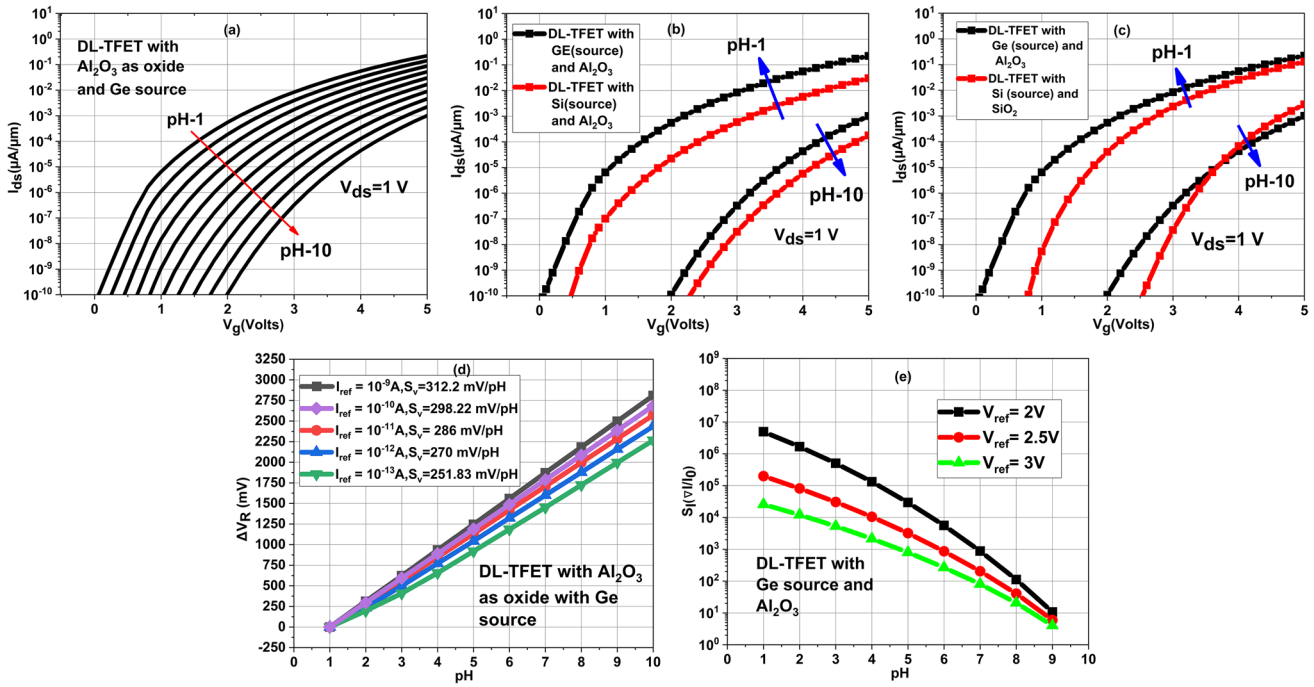

Fig. 7 (**a**) Drain current (I_{ds}) vs. gate voltage (V_g) as a function of pH varying from 1 to 10 for DL-TFET with Al_2O_3 as sensitive oxide layer having germanium as source doping material (**b**) Comparison of drain current vs. gate voltage at pH = 1 and 10 for DL-TFET with Al_2O_3 for both variant having silicon and germanium as source material (**c**) Comparison of transfer curve at pH = 1 and 10 for germanium source based DL-TFET having Al_2O_3 as sensitive layer and silicon source based DL-TFET having SiO_2 as sensitive layer (**d**) Variation of responsive gate voltage (ΔV_R) with pH for drain current (I_{ref}) of 10^{-9} A, 10^{-10} A, 10^{-11}A, 10^{-12} and 10^{-13}A for germanium source based DL-TFET with Al_2O_3 as sensitive layer (**e**) Variation of S_I with pH for gate voltage (V_{ref}) of 2 V, 2.5 V and 3 V for DL-TFET with Al_2O_3 as underlapped oxide layer and germanium source

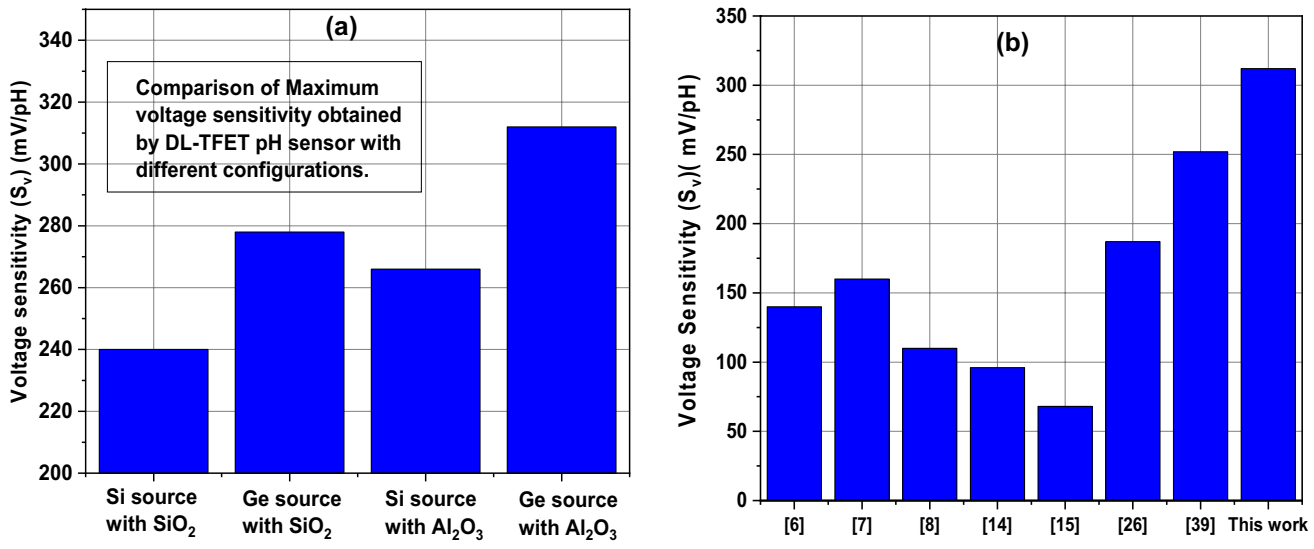

Fig. 8 (**a**) Comparison of maximum voltage sensitivity (S_V) achieved by DL-TFET device with different configurations. (**b**) Comparison of voltage sensitivity of this work with previously reported work

4 Conclusion

In this work detailed simulation-based study of doping less TFET device having source sided underlapped region is done. It is sensitive to pH variations in an aqueous electrolyte environment. The results are also compared with conventional TFET device with same configuration. The findings demonstrate that the DL-TFET based device can be preferred over the conventional doped TFET based device for the use of pH sensing applications as they provide same sensitivity with benefits of reduced fabrication complexity and immunity against RDF as well. Moreover, use of high-K dielectric oxides and low energy band gap material like germanium can significantly increase the device sensitivity. The maximum sensitivity achieved in this work is 312 mV/pH which is more than the 5 times of Nernstian limit.

Author's Contributions Zuber Rasool: Simulation, Computation, TCAD software and Writing – Original draft preparation.

S. Intekhab Amin: Conceptualization, Computation, TCAD software, Revision, Supervision, and Validation.

Lubna Majeed: Computation, TCAD software Simulation and Writing.

Ishrat Bashir: Simulation and Writing.

Anjar Seraj: Computation and simulation.

Sunny Anand: revision, Supervision, and Validation.

Funding The authors declare that no funds, grants, or other support received during the preparation of this manuscript.

Data Availability Not Applicable.

Declarations

Ethics Approval and Consent to Participate Not Applicable.

Consent for Publication Not Applicable.

Informed Consent Not Applicable.

Research Involving Human Participants and/or Animals Not Applicable.

Disclosure of Potential Conflicts of Interest No conflicts of interest to report.

Competing Interests The authors declare no competing interests.

References

1. Bergveld P (1970) Development of an ion-sensitive solid-state device for neurophysiological measurements. IEEE Trans Biomed Eng 17(1):70–71. https://doi.org/10.1109/DRC.2012.6256950
2. Bergveld P (1986) The development and application of FET-based biosensors. Biosensors 2(1):15–33. https://doi.org/10.1016/0265-928x(86)85010-6
3. Kim C-H, Jung C, Lee K-B, Park HG, Choi Y-K (2011) Label-free DNA detection with a nanogap embedded complementary metal oxide semiconductor. Nanotechnology 22(13):135502. https://doi.org/10.1088/0957-4484/22/13/135502
4. Chen X et al (2010) () Electrical nanogap devices for biosensing. Mater Today (Kidlington) 13(11):28–41. https://doi.org/10.1016/S1369-7021(10)70201-7
5. van Hal REG, Eijkel JCT, Bergveld P (1995) A novel description of ISFET sensitivity with the buffer capacity and double-layer capacitance as key parameters. Sens Actuators B Chem 24(1–3):201–205. https://doi.org/10.1016/0925-4005(95)85043-0
6. Reddy B Jr et al (2011) High-k dielectric Al_2O_3 nanowire and nanoplate field effect sensors for improved pH sensing. Biomed Microdevices 13(2):335–344. https://doi.org/10.1007/s10544-010-9497-z
7. Liu N, Hui Liu Y, Feng P, Qiang Zhu L, Shi Y, Wan Q (2015) Enhancing the pH sensitivity by laterally synergic modulation in dual-gate electric-double-layer transistors. Appl Phys Lett 106(7):073507. https://doi.org/10.1063/1.4913445
8. Ahn J-H et al (2013) A pH sensor with a double-gate silicon nanowire field-effect transistor. Appl Phys Lett 102(8):083701. https://doi.org/10.1063/1.4793655
9. Baek DJ, Duarte JP, Moon D-I, Kim C-H, Ahn J-H, Choi Y-K (2012) Accumulation mode field-effect transistors for improved sensitivity in nanowire-based biosensors. Appl Phys Lett 100(21):213703. https://doi.org/10.1063/1.4723843
10 Spijkman M, Smits ECP, Cillessen JFM, Biscarini F, Blom PWM, de Leeuw DM (2011) Beyond the Nernst-limit with dual-gate ZnO ion-sensitive field-effect transistors. Appl Phys Lett 98(4):043502. https://doi.org/10.1063/1.3546169
11. Jang H-J, Cho W-J (2012) Fabrication of high-performance fully depleted silicon-on-insulator based dual-gate ion-sensitive field-effect transistor beyond the Nernstian limit. Appl Phys Lett 100(7):073701. https://doi.org/10.1063/1.3685497
12. Sarkar D, Banerjee K (2012) Fundamental limitations of conventional-FET biosensors: Quantum-mechanical-tunneling to the rescue. In: 70th Device Research Conference. University Park, PA, pp 83–84. https://doi.org/10.1109/DRC.2012.6256950
13 Go J, Nair PR, Reddy B Jr, Dorvel B, Bashir R, Alam MA (2012) Coupled heterogeneous nanowire-nanoplate planar transistor sensors for giant (>10 V/pH) Nernst response. ACS Nano 6(7):5972–5979. https://doi.org/10.1021/nn300874w
14. Knopfmacher O et al (2010) Nernst limit in dual-gated Si-nanowire FET sensors. Nano Lett 10(6):2268–2274. https://doi.org/10.1021/n1100892y
15. Kumar N, Kumar J, Panda S (2016) Enhanced pH sensitivity over the Nernst limit of electrolyte gated a-IGZO thin film transistor using branched polyethylenimine. RSC Adv 6(13):10810–10815. https://doi.org/10.1039/c5ra26409j
16. Go J, Nair PR, Reddy B, Dorvel B, Bashir R, Alam MA (2010) Beating the Nernst limit of 59mV/pH with double-gated nanoscale field-effect transistors and its applications to ultra-sensitive DNA biosensors. In: 2010 International Electron Devices Meeting. San Francisco, CA, pp 8.7.1–8.7.4. https://doi.org/10.1109/IEDM.2010.5703325
17. Cao W, Sarkar D, Khatami Y, Kang J, Banerjee K (2014) Subthreshold-swing physics of tunnel field-effect transistors. AIP Adv 4(6):067141
18 Ionescu AM, Riel H (2011) Tunnel field-effect transistors as energy-efficient electronic switches. Nature 479(7373):329–337. https://doi.org/10.1038/nature10679
19. Sarkar D, Banerjee K (2012) Proposal for tunnel-field-effect-transistor as ultra-sensitive and label-free biosensors. Appl Phys Lett 100(14):143108. https://doi.org/10.1063/1.3698093
20. Bal P, Akram MW, Mondal P, Ghosh B (2013) Performance estimation of sub-30 nm junctionless tunnel FET (JLTFET).

J Comput Electron 12(4):782–789. https://doi.org/10.1007/s10825-013-0483-6
21. Leung G, Chui CO (2012) Variability Impact of Random Dopant Fluctuation on Nanoscale Junctionless FinFETs. IEEE Electron Device Lett 33(6):767–769. https://doi.org/10.1109/LED.2012.2191931
22 Kumar MJ, Janardhanan S (2013) Doping-less tunnel field effect transistor: Design and investigation. IEEE Trans Electron Devices 60(10):3285–3290. https://doi.org/10.1109/TED.2013.2276888
23. Anand S, Amin SI, Sarin RK (2016) Performance analysis of charge plasma based dual electrode tunnel FET. J Semicond 37(5):054003. https://doi.org/10.1088/1674-4926/37/5/054003
24. Anand S, Singh A, Amin SI, Thool AS (2019) Design and performance analysis of dielectrically modulated doping-less tunnel FET-based label free biosensor. IEEE Sens J 19(12):4369–4374
25. Wadhwa G, Raj B (2018) Label free detection of biomolecules using charge-plasma-based gate underlap dielectric modulated junctionless TFET. J Electron Mater 47(8):4683–4693
26 Dwivedi P, Singh R, Chauhan YS (2021) Crossing the Nernst limit (59 mV/pH) of sensitivity through tunneling transistor-based biosensor. IEEE Sens J 21(3):3233–3240. https://doi.org/10.1109/JSEN.2020.3025975
27. Silvaco International (2021) Atlas user's manual: device simulation software, Version 5.2.14.R. Silvaco Int. Inc., Santa Clara, CA
28. Lee B-S et al (2021) Doping-less tunnel field-effect transistors by compact Si drain frame/Si0.6Ge0.4-channel/Ge source. AIP Adv. 11(4):045007
29 Bandiziol A, Palestri P, Pittino F, Esseni D, Selmi L (2015) A TCAD-Based Methodology to Model the Site-Binding Charge at ISFET/Electrolyte Interfaces. IEEE Trans Electron Devices 62(10):3379–3386. https://doi.org/10.1109/TED.2015.2464251
30. Choi B et al (2015) TCAD-Based Simulation Method for the Electrolyte–Insulator–Semiconductor Field-Effect Transistor. IEEE Trans Electron Devices 62(3):1072–1075. https://doi.org/10.1109/TED.2015.2395875
31. Pittino F, Palestri P, Scarbolo P, Esseni D, Selmi L (2014) Models for the use of commercial TCAD in the analysis of silicon-based integrated biosensors. Solid State Electron 98:63–69. https://doi.org/10.1016/j.sse.2014.04.011
32 Kannan N, Kumar MJ (2015) Charge-modulated underlap I-MOS transistor as a label-free biosensor: A simulation study. IEEE Trans Electron Devices 62(8):2645–2651. https://doi.org/10.1109/TED.2015.2446612
33. Koneshan S, Rasaiah JC, Lynden-Bell RM, Lee SH, Lynden-Bell RM, Lee SH (1998) Solvent structure, dynamics, and ion mobility in aqueous solutions at 25 °C. J Phys Chem B 102(98):4193–4204. https://doi.org/10.1021/jp980642x
34 Yates DE, Levine S, Healy TW (1974) Site-binding model of the electrical double layer at the oxide/water interface. J Chem Soc 70:1807
35 Bousse L, De Rooij NF, Bergveld P (1983) Operation of chemically sensitive field-effect sensors as a function of the insulator-electrolyte interface. IEEE Trans Electron Devices 30(10):1263–1270. https://doi.org/10.1109/t-ed.1983.21284
36. Lee J, Hwang S, Choi B, Lee JH, Moon DI, Seol ML, Kim CH, Chung IY, Park BG, Choi YK, Kim DM, Kim DH, Choi SJ (2013) A novel SiNW/CMOS hybrid biosensor for high sensitivity/low noise. In: 2013 IEEE International Electron Devices Meeting. IEEE, Washington, DC, pp 14.5.1–14.5.4. https://doi.org/10.1109/IEDM.2013.6724631
37. Bedner K et al (2010) pH response of silicon nanowire sensors: Impact of nanowire width and gate oxide. Sensors Mater 25(8):567–576
38 Narang R, Saxena M, Gupta M (2017) Analytical model of pH sensing characteristics of junctionless silicon on insulator ISFET. IEEE Trans Electron Devices 64(4):1742–1750. https://doi.org/10.1109/TED.2017.2668520
39 Nakazawa H, Otake R, Futagawa M, Dasai F, Ishida M, Sawada K (2014) High-sensitivity charge-transfer-type pH sensor with quasi-signal removal structure. IEEE Trans Electron Devices 61(1):136–140. https://doi.org/10.1109/TED.2013.2292563